THE JOURNAL OF BIOLOGICAL CHEMISTRY Vol. 276, No. 42, Issue of October 19, pp. 38995–39001, 2001
Printed in U.S.A.

The Mechanism of Superoxide Scavenging by *Archaeoglobus fulgidus* Neelaredoxin*

Received for publication, April 11, 2001, and in revised form, July 27, 2001
Published, JBC Papers in Press, August 6, 2001, DOI 10.1074/jbc.M103232200

Isabel A. Abreu‡§, Lígia M. Saraiva‡, Cláudio M. Soares‡, Miguel Teixeira‡¶, and Diane E. Cabelli‖

From the ‡Instituto de Tecnologia Química e Biológica, Universidade Nova de Lisboa, Rua da Quinta Grande 6, APT 127, 2780-156 Oeiras, Portugal, and ‖Chemistry Department, Brookhaven National Laboratory, Upton, New York 11973-5000

Neelaredoxin is a mononuclear iron protein widespread among prokaryotic anaerobes and facultative aerobes, including human pathogens. It has superoxide scavenging activity, but the exact mechanism by which this process occurs has been controversial. In this report, we present the study of the reaction of superoxide with the reduced form of neelaredoxin from the hyperthermophilic archaeon *Archaeoglobus fulgidus* by pulse radiolysis. This protein reduces superoxide very efficiently ($k = 1.5 \times 10^9$ M^{-1}s^{-1}), and the dismutation activity is rate-limited, in steady-state conditions, by the much slower superoxide oxidation step. These data show unambiguously that the superfamily of neelaredoxin-like proteins (including desulfoferrodoxin) presents a novel type of reactivity toward superoxide, a result of particular relevance for the understanding of both oxygen stress response mechanisms and, in particular, how pathogens may respond to the oxidative burst produced by the defense cells in eukaryotes. The actual *in vivo* functioning of these enzymes will depend strongly on the cell redox status. Further insight on the catalytic mechanism was obtained by the detection of a transient intermediate ferric species upon oxidation of neelaredoxin by superoxide, detectable by visible spectroscopy with an absorption maximum at 610 nm, blue-shifted ~50 nm from the absorption of the resting ferric state. The role of the iron sixth ligand, glutamate-12, in the reactivity of neelaredoxin toward superoxide was assessed by studying two site-directed mutants: E12Q and E12V.

The scavenging of superoxide ($O_2^{\cdot-}$) by living cells is generally performed by superoxide dismutases (SODs)[1] of the Mn, Fe, CuZn, or Ni types. However, both biochemical data and the analysis of the entire genomes now available show that numerous prokaryotes do not contain any of those canonical SODs. Instead, they contain genes encoding for members of a novel family of $O_2^{\cdot-}$ scavengers (1–5) initially named neelaredoxin (Nlr) and desulfoferrodoxin (Dfx). These proteins share an unusual iron center, Fe(His_4Cys) (6–8), responsible for their reactivity with $O_2^{\cdot-}$. The Nlr from *Archaeoglobus fulgidus* exhibits an apparent bifunctional activity toward $O_2^{\cdot-}$: a superoxide reductase activity, using a flavoprotein (an NADH:Nlr oxidoreductase) as its electron donor, and a superoxide dismutase activity. The latter characteristic can be used by the organism to detoxify $O_2^{\cdot-}$ independently of the cell redox status (9). This novel family of $O_2^{\cdot-}$ scavengers is of utmost relevance because it is present in almost all anaerobes for which the complete genome sequence is known, as well as in several facultative aerobes, including human pathogens such as *Treponema pallidum*, the causative agent of syphilis (10). In many of these prokaryotes, these are the only types of $O_2^{\cdot-}$ scavengers present, *i.e.* the canonical SODs are absent. This observation is most important due to the relevance of $O_2^{\cdot-}$ scavenging as a defense mechanism not only of living cells, in general, but also, in particular, in the response of pathogens to the oxidative burst produced by the host defense cells. To understand this process at the molecular level, it is essential to start by unraveling the catalytic mechanism of these novel enzymes. Toward this goal, the reactivity of reduced Nlr from *A. fulgidus* with $O_2^{\cdot-}$ was studied by pulse radiolysis. The active centers in both Dfx and Nlr are very similar, but they behave in some strikingly different fashions. Dfx is isolated with the $O_2^{\cdot-}$ active iron as Fe^{2+}, whereas Nlr is isolated mainly in the Fe^{3+} form. In addition, they appear to have different reactivities toward $O_2^{\cdot-}$ because Dfx is a superoxide reductase (SOR), and *A. fulgidus* Nlr is a bifunctional enzyme (both a dismutase and a reductase for $O_2^{\cdot-}$). Recently, a mechanism for the reduction of $O_2^{\cdot-}$ by Dfx was proposed (11), which, together with this study, makes it possible to compare the reactivity of both enzymes toward $O_2^{\cdot-}$, an essential step for understanding the overall catalytic mechanism of these new types of $O_2^{\cdot-}$ scavengers. In particular, Nlr offers the advantage over Dfx of having a single iron center, allowing probing of the intrinsic reactivity of only that center, without any possible interference from the other center present in Dfx.

The three-dimensional structure of *Pyrococcus furiosus* Nlr (8) suggests that the iron coordination changes with the protein redox state. In the oxidized form, the iron center has an octahedral geometry, with four planar histidine ligands and one cysteine and a glutamate as axial ligands. In the reduced form, the glutamate is not bound to the iron, which becomes five coordinated in a square pyramidal geometry. This coordination is similar to that of center II in Dfx (7). The binding of the sixth ligand (E14, in *P. furiosus*) to the oxidized form was suggested to limit access of the $O_2^{\cdot-}$ to this redox state of the metal (8). However, Nlr from *A. fulgidus* shows superoxide dismutase activity (9), and this reactivity implies access of $O_2^{\cdot-}$ to both the reduced and oxidized forms of the iron. It is possible that the glutamate is somehow controlling the reactivity of Nlr, but it can also be argued that the oxidation of $O_2^{\cdot-}$ can be accomplished

* This work was supported in part by Fundação para Ciência e Tecnologia (Portugal) Projects 32789/99 and 36558/99. The costs of publication of this article were defrayed in part by the payment of page charges. This article must therefore be hereby marked "*advertisement*" in accordance with 18 U.S.C. Section 1734 solely to indicate this fact.
§ Supported by PraxisXXI.
¶ To whom correspondence may be addressed. Tel.: 351-214469844; Fax: 351-214468766; E-mail: miguel@itqb.unl.pt.
** To whom correspondence may be addressed. Tel.: 631-344-4361; E-mail: cabelli@bnl.gov.
[1] The abbreviations used are: SOD, superoxide dismutase; Nlr, neelaredoxin; Dfx, desulfoferrodoxin; SOR, superoxide reductase.

by an outer sphere electron transfer. *A. fulgidus* Nlr has a glutamate residue (E12) in an equivalent position to the E14 from *P. furiosus* Nlr. Moreover, this is a conserved residue in all known Nlrs and Dfxs (9), suggesting a functional role for this residue. To assess the role of the glutamate, a sixth ligand of the ferric state of the iron center, two mutants were also analyzed in which this residue was substituted by either a valine (E12V) or a glutamine (E12Q).

EXPERIMENTAL PROCEDURES

Expression and Purification of Recombinant Neelaredoxin Mutants

Construction of Escherichia coli Transformants for the Expression of Neelaredoxin Mutants—A pT7-7 plasmid containing the Nlr gene (pT7AfNlr) (9) was used as a template in a site-directed mutagenesis assay to create an E12V and an E12Q mutation in Nlr (plasmids pT7AfNlrE12V and pT7AfNlrE12Q), using the QuikChange™ Site-directed Mutagenesis kit from Stratagene. The generated nicked vector DNA incorporating the desired mutations was then repaired by transformation in *E. coli* XL-2 Blue (Stratagene). After plasmid isolation, the plasmids were sequenced to confirm the presence of the desired mutation and the absence of any unwanted one. Samples were prepared using the ABI PRISM Dye Terminator Cycle Sequencing kit (PerkinElmer Life Sciences) as per the manufacturer's instructions and run in an Applied Biosystems 373A DNA Sequencer. For the expression experiments, plasmids pT7AfNlr, pT7AfNlrE12V, and pT7AfNlrE12Q were introduced in *E. coli* BL21-Gold(DE3)pLysS cells (Stratagene).

Cell Growth—Recombinant *E. coli* cells were aerobically grown at 37 °C in Luria-Bertani medium supplemented with 100 μg/ml^{-1} ampicillin in a 3L fermentor. When the culture reached a cell density of A_{600} = 0.5, 1 mM isopropyl-1-thio-β-D-galactopyranoside was added, and after 9 h, the cells were harvested by centrifugation (10,000 × *g,* 10 min) and washed with 10 mM Tris-HCl, pH 7.0.

Protein Purification—The cells were broken in a French Press at 9000 p.s.i. The broken cells were centrifuged for 30 min at 10,000 × *g* to separate the cell debris, thus obtaining the crude extract. The crude extract was ultracentrifuged at 160,000 × *g* for 1 h, and the supernatant (soluble extract) was decanted. The supernatant was heated at 80 °C for 30 min and then centrifuged at 40,000 × *g* for 30 min. This treatment does not affect Nlr integrity or activity (9). The effects on Nlr mutants were tested, and the same results were obtained (this work; data not shown).

The heat-treated soluble extracts were purified in a Q-Sepharose column equilibrated with 10 mM Tris-HCl and eluted with a 0–0.5 M NaCl linear gradient in the same buffer. The fraction containing Nlr was then loaded in a HTP-ceramic column equilibrated with 5 mM potassium phosphate buffer and eluted with a 0–0.5 M potassium phosphate linear gradient. All purification steps were performed at pH 7.1 and 4 °C. The purity of the resulting Nlr was tested by SDS-polyacrylamide gel electrophoresis as described previously (12), and the bicinchoninic acid protein assay kit (Pierce) was used to determine protein concentration (13). Total iron content was determined by the 2,4,6-tripyridyl-*s*-triazine method as described previously (14) and by atomic absorption spectroscopy using a Pye-Unicam atomic absorption instrument. Zinc content was determined by atomic absorption spectroscopy. Measurements were made in triplicate with an experimental error of <5%. Iron and zinc content was determined for all proteins.

Throughout the text, the recombinant protein will be designated wild type Nlr, and the mutant proteins will be called NlrE12V and NlrE12Q. All activities are reported in relation to the iron content because zinc is not reactive with O_2^-. All kinetic data obtained are consistently proportional to the iron content of the samples, thus showing that there is no effect due to the presence of zinc. Moreover, the data now obtained are fully consistent with our previous preliminary kinetic study with fully iron-loaded enzyme (9).

Spectroscopic Studies

Room temperature UV-visible spectra were recorded on a Shimadzu UV-1603 spectrophotometer. EPR spectra were obtained on a Bruker ESP 380 spectrometer equipped with a continuous flow Oxford Instruments helium cryostat.

Redox titrations were performed under aerobic conditions and monitored by visible spectroscopy (400–820 nm), using a protein concentration sufficient to have a 660 nm band with at least 0.2 of absorbance. Nlr has a tendency to become re-reduced under anaerobic conditions, leading to redox titrations with a bad equilibrium. For this reason, we repeated all titrations under aerobic conditions, and as compared with our previously determined values (9), this does not affect the determination of the redox potential. The reaction mixture also contains a 2 μM final concentration of the following mediators: *N-N*-dimethyl-*p*-phenyldiamine (+340 mV), 1,2-naphtoquinone-4-sulfonic acid (+215 mV), 1,2-naphtoquinone (+180 mV), phenazine methosulfate (+80 mV), and 1,4-napthoquinone (+60 mV). The protein was mixed with the mediators and left under an argon atmosphere until fully reduced. The redox titration was then performed using potassium persulfate as oxidant. The redox potential measurements were done with a combined silver/silver chloride electrode calibrated with a quinhydrone-saturated solution at pH 7.0. The redox potentials are quoted against the standard hydrogen electrode.

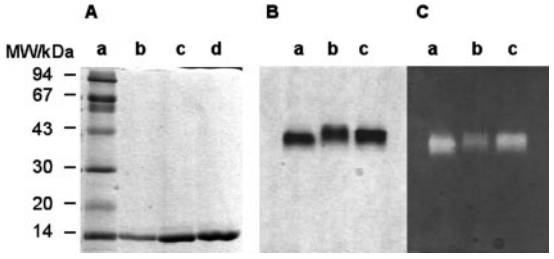

FIG. 1. *A,* SDS-polyacrylamide gel electrophoresis; Coomassie Blue staining of molecular mass markers (*a*), 3 μg of Nlr (*b*), 9 μg of NlrE12V (*c*), and 10 μg of NlrE12Q (*d*). *B,* 10 μg of Nlr (*a*), 10 μg of NlrE12V (*b*), and 10 μg of NlrE12Q (*c*) stained with Coomassie Blue. *C,* 10 μg of Nlr (*a*), 10 μg of NlrE12V (*b*), and 10 μg of NlrE12Q (*c*) stained with nitro blue tetrazolium.

Neelaredoxin Reactivity toward Superoxide

SOD Activity Assays—SOD activity was tested on nitro blue tetrazolium-stained gels, as described in Ref. 15. The Nlr SOD activity was quantified by the standard xanthine/xanthine oxidase method, where 1 activity unit is defined as the amount of enzyme necessary to inhibit 50% of the reduction of cytochrome *c* by the xanthine/xanthine oxidase system (15).

Pulse Radiolysis Assays—Pulse radiolysis experiments were carried out using the 2 MeV Van de Graaff accelerator as described previously (16). Dosimetry was measured using the $(SCN)_2^-$ dosimeter (16). The radiolysis of water, either by electrons or γ-rays, yields the species described in Reaction 1, where the numbers in parentheses are G values, that is the number of molecules/100 eV of energy absorbed by the medium (17).

$$H_2O \rightsquigarrow e_{aq}^-(2.75), OH(2.65), H(0.65), H_2O_2(0.7)\ H_2(0.45) \quad (1)$$

The species can be converted to secondary radicals, depending on the presence of adequate scavengers. In aerated solutions containing formate (HCO_2^-), primary radicals are converted to O_2^- by Reactions 2–4 (18).

$$e_{aq}^- + O_2 \rightarrow O_2^-\ pK(HO_2/O_2^-) = 4.8 \quad (2)$$

$$OH/H + HCO_2^- \rightarrow H_2O/H_2 + CO_2^- \quad (3)$$

$$CO_2^- + O_2 \rightarrow O_2^- + CO_2 \quad (4)$$

If the dioxygen is substituted by N_2O in the presence of formate instead of O_2^-, all primary species are converted to CO_2^- by Reactions 5 and 6.

$$e_{aq}^- + N_2O \rightarrow N_2 + O^- \xrightarrow{H_2O} OH + OH^- + N_2 \quad (5)$$

$$OH/H + HCO_2^- \rightarrow H_2O/H_2 + CO_2^- \quad (6)$$

All pulse radiolysis samples were prepared using Millipore ultrapurified distilled water. EDTA and sodium formate were of the highest purity commercially available and were used as purchased.

Reduced enzyme was obtained by the addition of stoichiometric quantities of ascorbate to a solution of Nlr. An additional method for preparation of reduced enzyme involved using a 1800 Curie ^{60}Co γ-ray source. The solution of Nlr was prepared in a N_2O atmosphere and in the presence of formate as ·OH scavenger, as described in Reactions 5

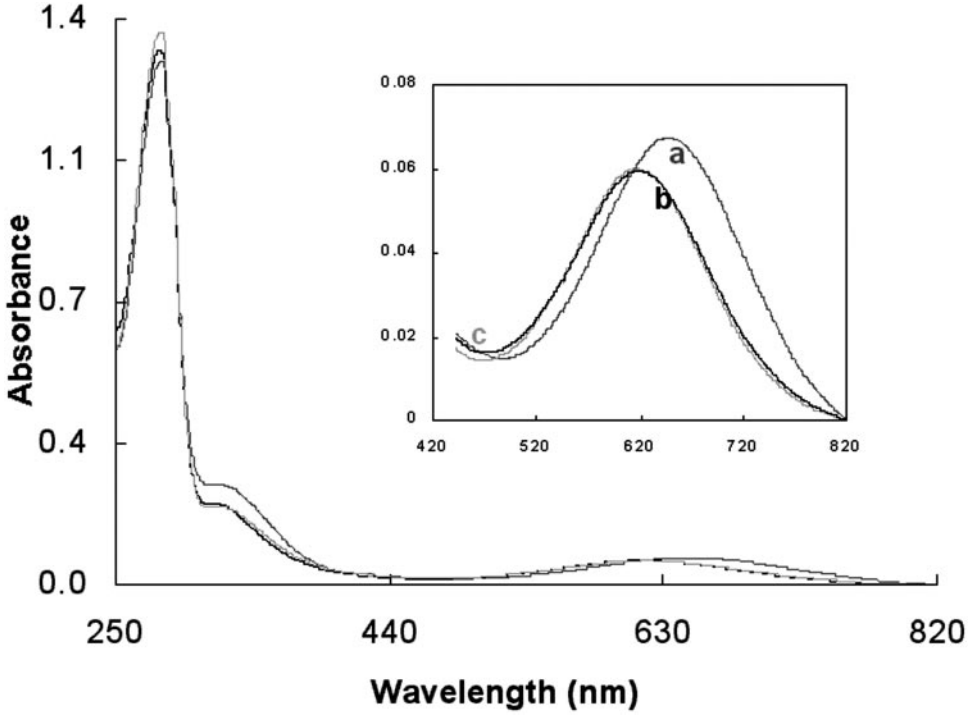

FIG. 2. UV-visible spectra of Nlr, NlrE12Q, and NlrE12V (57 μM). *Inset,* detailed view of the blue band of the proteins: *a,* Nlr; *b,* NlrE12Q; and *c,* NlrE12V.

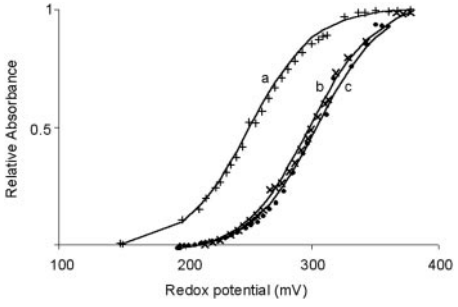

FIG. 3. **Redox titration of (*a*) Nlr, (*b*) NlrE12Q, and (*c*) NlrE12V.** The titration curves were obtained measuring the absorbance at 660 nm (+) for Nlr and at 620 nm (*X* and ●) for the mutant proteins NlrE12Q and NlrE12V, respectively; the *lines* correspond to Nernst equations with $n = 1$ and $E^o = +250$ mV for Nlr, $E^o = +298$ mV for NlrE12Q, and $E^o = +302$ mV for NlrE12V.

and 6. Stoichiometric amounts of CO_2^- radicals were generated at a rate of ~1 μmol/s.

Molecular Modeling

The very high identity between the sequences of *A. fulgidus* and *P. furiosus* Nlr (67% sequence identity) is an indication that the structural model of *A. fulgidus* Nlr obtained on the basis of the structure of the protein from *P. furiosus* will be close to the real structure. It is considered (19, 20) that, for sequence identities above 60%, the modeled structure may be as good as a medium resolution NMR structure or a low resolution x-ray structure. For highly conserved zones, such as the metal site of Nlr, this quality can be even higher.

The program Modeller version 4 (21) was used to derive the tetramer models for the oxidized and reduced forms of *A. fulgidus* Nlr from the corresponding structures of *P. furiosus* Nlr (8) (Protein Data Bank codes 1DQI and 1DQK). The initial sequence alignment was optimized to yield structural models with correct conformational characteristics; these were checked using PROCHECK (22). Using the final optimized alignment, 40 structures were generated by Modeller (for the oxidized and reduced states). The structure with the lowest value of the objective function was chosen. In the case of the oxidized structure model, the zone of K10 (W9-K10-K11) was optimized further (loop modeling in Modeller) in the framework of the rest of the structure to generate a conformation outside of the main chain forbidden zones. The final models of the oxidized and reduced states had 90% and 89% of the residues, respectively, in most favored regions of the Ramachandran plot. None had residues in disallowed regions.

The mutant structures were obtained using the wild type structures and by mutation of the E12 residue using Sybyl 6.2 from TRIPOS. The resulting structures were minimized by considering residues 11–12-13 as flexible and considering the rest of the protein as rigid.

RESULTS

Preparation of Recombinant Neelaredoxin and Neelaredoxin Mutants (NlrE12Q and NlrE12V)—The potential sixth ligand for Nlr iron center (E12) was mutated to a glutamine (E12Q) and to a valine (E12V) by site-directed mutagenesis. Overexpression in *E. coli* produced stable proteins that were purified with comparable yields in the case of wild type Nlr and NlrE12Q (27 and 29 mg/liter^{-1}, respectively). The yield of NlrE12V was approximately one-third smaller (18 mg/liter^{-1}). The protein purity was confirmed by denaturing gel electrophoresis (SDS-polyacrylamide gel electrophoresis) (Fig. 1*A*). On a native gel electrophoresis, the proteins show a single band that corresponds to the SOD activity band obtained for nitro blue tetrazolium-stained gels (Fig. 1*B*). The proteins contain ~0.45 iron atom/monomer and roughly an equivalent amount of zinc. The rate data are reported in relation to the iron content. Both mutants are as stable as the wild type protein.

Physicochemical Characterization—The wild type Nlr has a characteristic UV-visible spectrum in the ferric state (9, 23), with a broad band at ~660 nm that gives the enzyme its blue color in solution, and a shoulder at ~325 nm (Fig. 2, trace a). The mutants show similar spectra, with a blue-shift of the 660 nm band to 617 nm in the case of NlrE12V and 620 nm in the case of NlrE12Q (Fig. 2, traces b and c). The EPR spectra of the proteins do not show any differences between the mutants and the wild type Nlr (data not shown).

Redox titrations monitored by visible spectroscopy were performed at pH 7.0, following the increase in absorbance at 660 nm in the wild-type enzyme and at 620 nm in the mutant enzymes. The data were adjusted to a Nernst equation ($n = 1$) with a reduction potential of +250 mV (Fig. 3, *a*) for the

TABLE I
Rate constants for the SOD activity determined with the xanthine/xanthine oxidase assay and for the reduction and oxidation steps, determined by pulse radiolysis of Nlr and neelaredoxin mutants (NlrE12Q and NlrE12V)

Sample	SOD activity	Reduction with CO_2^-	Oxidation with O_2^-	
		k(Nlr-Fe^{3+} + CO_2^- → Nlr-Fe^{2+})	k_1(Nlr-Fe^{2+} + O_2^- → T1)	k_2(T1 → Nlr-Fe^{3+})
	(units/mg^{-1})	*($\times 10^8$/M^{-1} s^{-1})*	*($\times 10^9$/M^{-1} s^{-1})*	*($\times 10^4$/s^{-1})*
Nlr	78 ± 8	5.9 ± 0.7	1.5 ± 0.5	
NlrE12Q	101 ± 13	4.0 ± 1.8	1.5 ± 0.3	~2
NlrE12V	115 ± 28	1.9 ± 0.5	0.4 ± 0.03	

wild-type enzyme, +298 mV for NlrE12Q (Fig. 3, *b*), and +302 mV for NlrE12V (Fig. 3, *c*). This increase in reduction potential is in agreement with the removal of an anionic ligand, the glutamate, that stabilizes the ferric state. The structure of the *P. furiosus* protein suggests that Nlr is a tetramer with four iron centers (one iron center/monomer). Although equal, these centers can in theory feel the influence of each other and, as a consequence, produce a perturbation in the their redox behavior. However, given the large distances between the centers (about 25 Å) and their high solvent exposure, direct electrostatic influences will be small (due to their fast decay with distance in solvent environments), and therefore the mutual influence in microscopic redox potentials will be very reduced. The result is that all four iron centers are equivalent, and when being titrated, the experimental values can be fitted to a single Nernst equation.

SOD Activity—The xanthine/xanthine oxidase assay shows a 47% and 29% increase in the activities of the NlrE12V and NlrE12Q, respectively, relative to the activity of the wild type enzyme (Table I). This increase suggests a role for the glutamate residue in the regulation of SOD activity in Nlr.

Pulse radiolysis experiments were carried out under conditions in which the primary radicals are mainly converted to CO_2^- (Reactions 5 and 6), leading to the reduction of Nlr's iron center. The disappearance of the Fe^{3+} band was followed at a range of wavelengths from 400 nm to 700 nm on the microsecond time scale, and a difference spectrum was generated. The extinction coefficients were calculated assuming that 100% of the CO_2^- reacts to reduce Nlr-Fe^{3+} to Nlr-Fe^{2+}; CO_2^- is known not to absorb in this spectral region. The experimental data were fitted to a simple first-order kinetic process (Fig. 4*B*). Using 10–300 μM Fe^{3+}-protein and generating 1–2 μM CO_2^- by pulse radiolysis, the wild type and the mutant enzymes react with CO_2^- at ~10^8 M^{-1} s^{-1}, although NlrE12V has a slightly slower reactivity when compared with the other proteins (Table I). The wild type Nlr has a difference spectrum with a maximum at ~660 nm (Fig. 4), and the mutant proteins have spectra with maxima at ~620 nm, as expected from the respective absorption spectra (Fig. 2).

The proteins were reduced to 99% using the steady-state generation of CO_2^- in a ^{60}Co source, with formate as a OH· scavenger and N_2O as the electron scavenger. The reduced samples were then saturated with O_2 and pulsed to generate O_2^-. The re-oxidation of Fe^{2+} in the proteins by O_2^- is not a simple process (Fig. 4*A*). The change in absorbance with time was fitted to two first-order processes, where the initial process occurred at a rate that was proportional to the initial Fe^{2+} concentration, and the subsequent process occurred at a rate that was independent of both O_2^- and Nlr concentration. This indicates the existence of a transient intermediate. The calculated rate constants for both processes in the wild type enzyme and mutants are presented in Table I. The observed absorption changes are consistent with a mechanism where O_2^- → intermediate → final species; thus, spectra of the intermediate and final species can be calculated for the

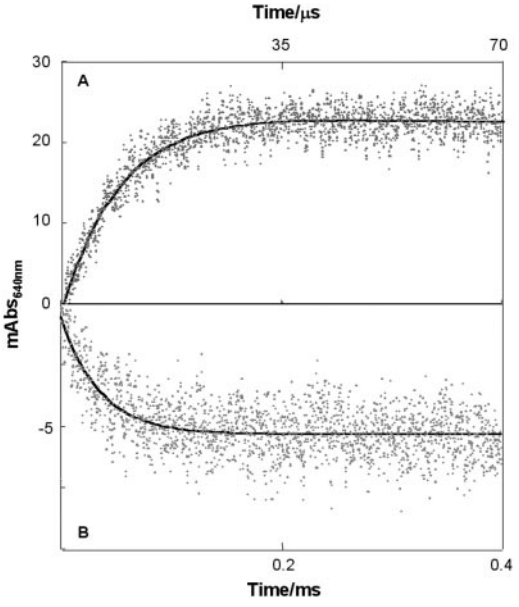

FIG. 4. Time courses for the oxidation of neelaredoxin after reduction in a 1800 Curie ^{60}Co γ-ray source (*A*) with O_2^- and for the reduction of neelaredoxin with CO_2^- (*B*).

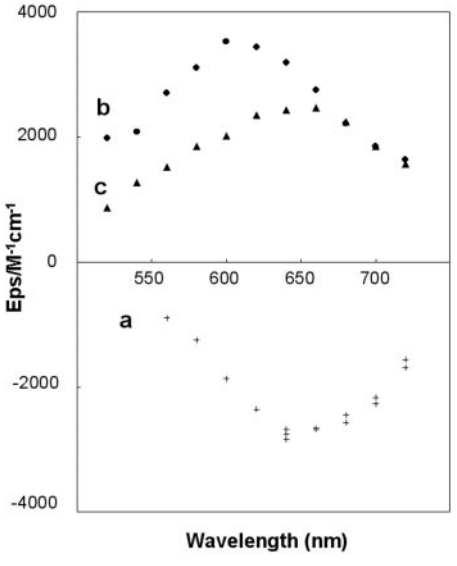

FIG. 5. Optical spectra of (*a*) reduced minus oxidized neelaredoxin, (*b*) 610 nm intermediate, and (*c*) final product.

three proteins. The intermediate species detected for both the wild type Nlr (Fig. 5) and NlrE12Q have spectra with absorption maxima at ~610 nm and show an increase in extinction coefficient. The spectrum of the intermediate is not so well defined in NlrE12V, but the kinetic evidence for its presence comes from studies of the re-oxidation process in which the kinetic traces can only be fitted by two consecutive first-order processes. The final species in all three proteins have spectra similar to that of the ferric state in the corresponding protein.

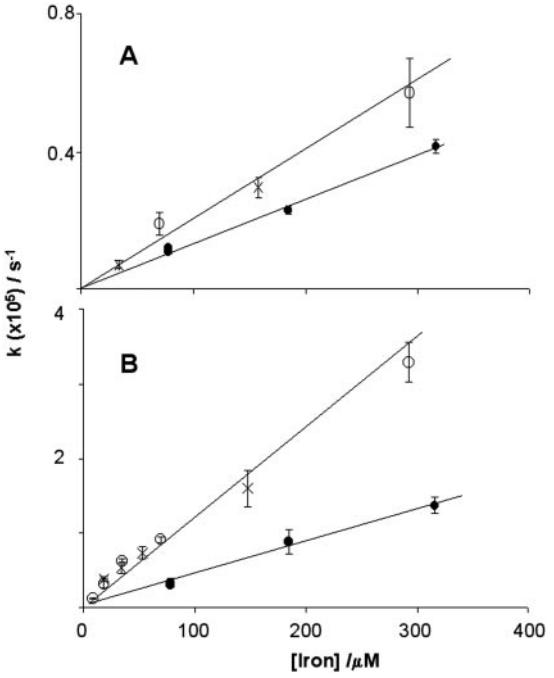

FIG. 6. **Linear dependence of rate constants for the reaction Nlr-Fe^{3+} + CO_2^- → Nlr-Fe^{2+} (*A*) and Nlr-Fe^{2+} + O_2^- → T1 (*B*) of neelaredoxin (*X*), NlrE12Q (○), and NlrE12V (●) with the concentration of iron in the proteins.** Neelaredoxin and NlrE12Q show the same behavior in both reactions. NlrE12V reacts slowly with superoxide and also shows a slight decrease in the reaction with CO_2^-.

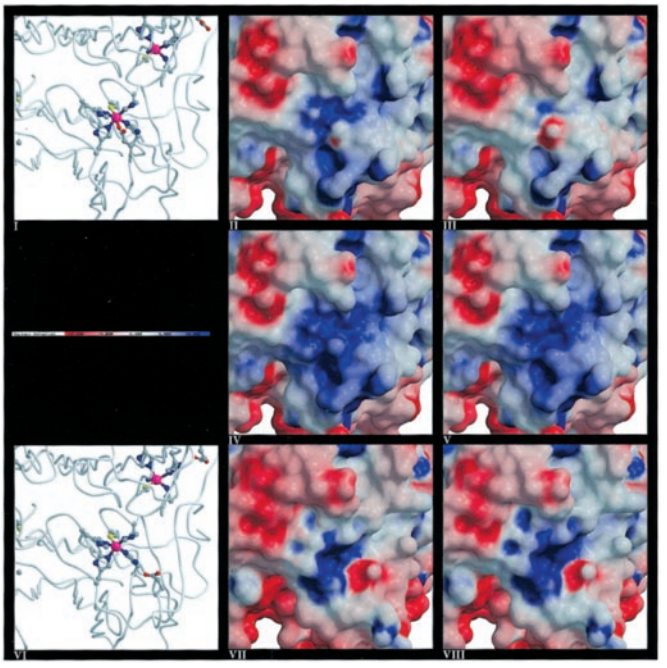

FIG. 7. **The model structure of *A. fulgidus* neelaredoxin.** *I,* close-up of the iron center in monomer A in the oxidized state. The iron and its ligands (including E12) are rendered using *ball and sticks,* whereas the rest of the protein is rendered using a Cα tracing. The iron center of monomer B is partially visible at the *upper right corner*. *II,* molecular surface of the oxidized structure in the same orientation as *I*. This surface, as well as the other ones presented in the figure, are colored according to the electrostatic potential. *Blue* and *red* zones correspond to positive and negative potentials, respectively. The potential ranges (as illustrated in the *potential bar* at the *left*) from −10 to 10 *k*T/*e*. *III,* molecular surface of the reduced state, obtained using the structure of the oxidized form (*i.e.* without the conformational change characteristic of the reduced form). *IV,* molecular surface of the E12Q mutant in the oxidized state. *V,* molecular surface of the E12V mutant in the oxidized state. *VI,* close-up of the iron center in monomer A in the reduced state (rendering as in *I*). *VII,* molecular surface of the reduced structure in the same orientation as *VI*. *VIII,* molecular surface of the oxidized state, obtained using the structure of the reduced form. These figures were prepared using Molscript (28), GRASP (29), and Raster 3D (30).

Experiments analogous to those described above were carried out on solutions in which the proteins were initially reduced by a 2:1 concentration of ascorbate. The results obtained were identical using both ascorbate and CO_2^- as reductants.

The rates for the reduction by CO_2^- and re-oxidation by O_2^- of the Fe center were measured using several concentrations of protein. In Fig. 6, the observed rates are plotted as a function of iron concentration. The rates for reduction of the oxidized iron by CO_2^- and the initial reaction in the oxidation of the reduced iron by O_2^- are directly proportional to the iron concentration, as would be expected ($v_{ox} = k_{ox} \times [Fe^{3+}] \times [CO_2^-]$ and $v_{red1} = k_{red1} \times [Fe^{2+}] \times [O_2^-]$, respectively). These measurements confirm that NlrE12Q has a behavior similar to the wild type enzyme, whereas NlrE12V shows a slower rate for both processes. The rate constant for the disappearance of the intermediate is, as expected, independent of the iron concentration ($v_{red2} = k_{red2} \times [T1]$) (data not shown).

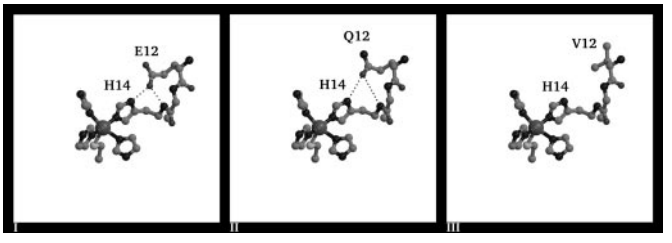

FIG. 8. **Close-ups of the *A. fulgidus* neelaredoxin iron center in the reduced state (monomer A).** The iron, its ligands, and residue 12 are rendered using *ball and sticks*. Potential hydrogen bonds are rendered using *dotted lines*. *I,* wild type center. *II,* center in the E12Q mutant. *III,* center in the E12V mutant. These figures were prepared using Molscript (28) and Raster 3D (30).

DISCUSSION

Neelaredoxin and desulfoferrodoxin belong to a family of proteins with the capacity of eliminating O_2^-. Their role is particularly important in anaerobes because they are present in all the known genomes from these organisms that lack canonical SODs. Their physiological relevance in the scavenging of O_2^- is confirmed with the demonstration of their capacity to complement *E. coli sodA*$^-$ *sodB*$^-$ (1, 24).

Having a single iron center, Nlr allows probing of the intrinsic reactivity of only that center, without any possible interference from the Fe(Cys_4) center present in Dfx. In this sense, it is possible to study the oxidation and reduction of O_2^- together or as independent reactions. The kinetic study of the SOR activity of *A. fulgidus* Nlr reported here shows the existence of a transient species during the reduction of O_2^- by Nlr-Fe^{2+}, leading us to propose the following general mechanism for the reactivity of Nlr with O_2^-.

$$O_2^- + 2H^+ + \text{Nlr-Fe}^{2+} \xrightarrow{k1} T \xrightarrow{k2} \text{Nlr-Fe}^{3+} + H_2O_2 \quad (7)$$

$$O_2^- + \text{Nlr-Fe}^{3+} \xrightarrow{k3} \text{Nlr-Fe}^{2+} + O_2 \quad (8)$$

In the presence of NADH and a NADH:Nlr oxidoreductase to reduce Nlr, the enzyme can eliminate O_2^- through Reaction 7, acting as a SOR. This will be very effective if a transient concentration of O_2^- is present in the cell upon oxidative stress. However,

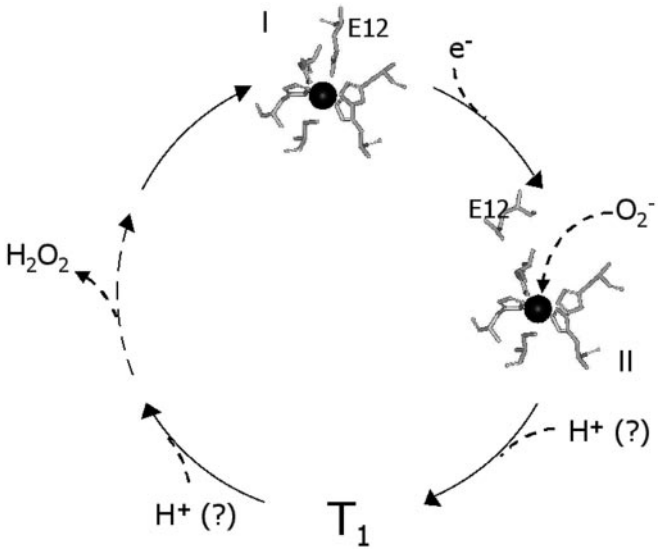

FIG. 9. **Catalytic cycle of superoxide reduction to hydrogen peroxide by neelaredoxin.** In the oxidized form of the protein (*I*), the glutamate (*E12*) is acting as a sixth ligand to the center, limiting the accessibility of superoxide to the iron. In these conditions, the oxidized center reacts slowly with superoxide, and this rate can be increased if the glutamate is substituted for a residue with less capability or no capability to bind the iron (NlrE12Q and NlrE12V, respectively). Upon reduction (*II*), the glutamate unbinds and establishes H-bonds to H14, determining the conformation of the active site groove. Superoxide can now react with the reduced iron in a rate diffusion-controlled manner because the center is exposed to the solvent. This rate is decreased if the glutamate is substituted for a residue without the capability of forming H-bonds (NlrE12V) because the right conformation of the reduced form of the center is not accomplished, but it is not affected when glutamate is substituted for a glutamine. The reduction of superoxide to hydrogen peroxide follows through the formation of a transient species (T_1), and the center becomes oxidized (*I*). The reduction of the iron center *in vivo* will be done through a Nlr:NAD(P)H oxidoreductase (9).

if the oxygen stress continues, the NAD^+:NADH ratio will rapidly increase (25), and Nlr will be oxidized by O_2^-. This oxidation, however, will not be complete because the enzyme will continue eliminating O_2^- by acting as a SOD (Reactions 7 and 8), albeit with a reduced rate constant (9). Interestingly, Nlr may not be the only bifunctional enzyme in its reactivity toward O_2^- because it was suggested that even canonical CuZn-SODs may act as SORs (26).

Recently, the reduction of O_2^- by the SORs (Dfxs) from *Desulfoarculus baarsii* and *Desulfovibrio vulgaris* was studied (11, 27), and in both cases, the oxidation of the Fe(Cys,His_4) center by O_2^- proceeded via formation of intermediate transient(s). We detect an analogous transient here, suggesting that oxidation of the iron center by O_2^- is independent of the presence of the Fe(Cys4) center in the SORs. Both the spectroscopic and kinetic data are unequivocal in establishing the presence of an intermediate, showing a transient species with a blue-shifted visible absorption and a dependence of the rate constants on the reactant concentrations that establishes the presence of an at least two-step reaction following re-oxidation of Nlr by O_2^-. The nature of the transient species for the reduction of O_2^- remains to be established. Its electronic properties (the absorbance band at 610 nm) indicate that the iron is in the ferric form and are similar to the oxidized state of the NlrE12 mutants (band at ~620 nm). The intermediate has been proposed to be a (hydro)peroxide-bound ferric iron (11). Although apparently sharing a common intermediate species during the reduction of O_2^-, Nlrs and Dfxs still exhibit important differences, namely, the rate constants for the various steps and the resting oxidation state of the enzyme when isolated *in vitro*. The initial reduction of O_2^- by the reduced enzyme (k1 in Reaction 7) is, in all cases, $\sim 10^9$ M^{-1} s^{-1}, but the rate of disappearance of the transient formed in that reaction (k2 in Reaction 7) is 3 orders of magnitude higher for Nlr than for *D. vulgaris* Dfx (2×10^4 s^{-1} and 40 s^{-1} (11), respectively). Recently, a second intermediate, which is apparently not present in Nlr or *D. vulgaris* Dfx, was reported for *D. baarsii* Dfx (27). In this protein, the first intermediate disappears at a rate of 500 s^{-1}, and the second intermediate disappears at a rate of 25 s^{-1}. Another significant difference between the mechanisms of Nlr and Dfx is in the O_2^- oxidation step. No SOD activity can be detected in pulse radiolysis studies of Dfx (11): when a considerable percentage of the Dfx Fe(Cys,His_4) center is reduced, only a stoichiometric reaction with O_2^- is observed, which disappears upon its oxidation (11), and no SOD activity is observed under catalytic conditions (where [Dfx] < [O_2^-]). Under the same conditions with Nlr, depending on the amount of reduced Fe(Cys,His_4) center, an initial fast reaction with O_2^- is observed. However, after the oxidation of the stoichiometric amount of reduced enzyme, there is a consistent rate constant of reaction with O_2^- that is the SOD activity of the enzyme (9). Under catalytic conditions, this rate is limited by that for the oxidation of O_2^- to O_2. The data now gathered also show that the Dfx Fe(Cys_4) center has no effect on the O_2^- reduction step, although by keeping the Fe(Cys,His_4) center reduced, it may have a role in promoting the O_2^- reduction reaction and thus eliminating the need for the O_2^- oxidation step.

The mutated Nlrs were designed to assess the influence of the binding of a sixth ligand (glutamate) to the iron, the influence of its negative charge, and the formation of H-bonds by the glutamate. Thus, this residue was replaced by glutamine, a neutral amino acid with the capacity of forming H-bonds, and a valine, with neither capacity to form H-bonds nor capacity to act as a sixth ligand. The UV-visible spectra of the mutated proteins show an equal blue-shift in the 660 nm band to ~620 nm, indicating that glutamate was replaced by a weaker ligand, possibly a water molecule. With regard to the O_2^- reduction step, the formation of the transient species and rate constants are similar for the wild type and NlrE12Q, but in the reduced form, NlrE12V reacts slower with O_2^- (Table I). In contrast, the SOD activity of the mutants increases (Table I). These results point to a role of the glutamate in the reaction mechanism of Nlr, as recently proposed (8), and can be discussed by analyzing the redox potentials of the proteins, their electrostatic characteristics, and the role of the H-bonds in determining the conformation of the active site groove in the reduced state. The increase in the reduction potential of the mutants may explain, in part, the higher activity of the O_2^- oxidation step. Also, because valine is not a ligand to the iron, the sixth position will be empty or occupied by a water molecule. Displacement of this weaker ligand will be easier than that of the glutamate ligand. The movement of the glutamate is essential to maintain the positive electrostatic potential at the iron center in both the oxidized (Fig. 7, *II*) and reduced (Fig. 7, *VII*) protein. The reduction of the iron without the conformational change induced by the unbinding of the glutamate gives a species (Fig. 7, *III*) with almost no positive electrostatic potential to direct the O_2^- to the center. Species VIII, obtained by modeling a Fe^{3+} center in the reduced form of the protein, is also less favorable to direct O_2^- to the iron than the oxidized protein, due to the dipole created by the glutamate side-chain. In the oxidized state, both mutants (Fig. 7, *IV* and *V*) have a more positive electrostatic surface around the iron because an anionic amino acid is substituted by neutral ones, which also contributes to the higher SOD activity of the mutants.

The differences observed in the SOR activities may be explained by considering a differential conformation of the reduced state: the open conformation of the reduced center is

fixed in both the wild type and E12Q proteins by H-bonds established by the sixth ligand with the H14, but this is not possible when glutamate is substituted by valine (Fig. 8). This would explain the decrease in the SOR activity for only the E12V mutant and not for E12Q. In this sense, the role of a sixth ligand with this capacity is important because it assures the accessibility of the O_2^- to the reduced iron center (Fig. 9).

In summary, *A. fulgidus* Nlr is an efficient SOR that belongs to a new family of O_2^- scavengers that are widespread among prokaryotes.

Acknowledgments—We thank Júlia Lobato (Instituto Gulbenkian Ciência) for DNA sequencing. Pulse radiolysis studies were carried out at the Center for Radiation Chemistry Research at Brookhaven National Laboratory, which is supported under contract DE-AC02–98CH109916 with the United States Department of Energy and supported by its Division of Chemical Science, Office of Basic Energy Sciences.

REFERENCES

1. Pianzzola, M. J., Soubes, M., and Touati, D. (1996) *J. Bacteriol.* **178,** 6736–6742
2. Romão, C. V., Liu, M.-Y., LeGall, J., Gomes, C. M., Braga, V., Pacheco, I., Xavier, A. V., and Teixeira, M. (1999) *Eur. J. Biochem.* **261,** 438–443
3. Silva, G., Oliveira, S., Gomes, C. M., Paheco, I., Liu, M.-Y., Xavier, A. V., Teixeira, M., LeGall, J., and Rodrigues-Pousada, C. (1999) *Eur. J. Biochem.* **259,** 235–243
4. Jenney, F. E., Jr., Verhgen, M. F. J. M., Cui, X., and Adams, M. W. W. (1999) *Science* **286,** 306–309
5. Lombard, M., Fontecave, M., Touati, D., and Nivière, V. (2000) *J. Biol. Chem.* **275,** 115–121
6. Moura, I., Tavares, P., Moura, J. J. G., Ravi, N., Huynh, B. H., Liu, M. Y., and Le Gall, J. (1990) *J. Biol. Chem.* **265,** 21596–21602
7. Coelho, A. V., Matias, P., Fülöp, V., Thompson, A., Gonzalez, A., and Carrondo, M. A. (1997) *J. Biol. Inorg. Chem.* **2,** 680–689
8. Yeh, A. P., Hu, Y., Jenney, F. E., Jr., Adams, M. W., and Rees, D. C. (2000) *Biochemistry* **39,** 2499–2508
9. Abreu, I. A., Saraiva, L. M., Carita, J., Huber, H., Stetter, K. O., Cabelli, D., and Teixeira, M. (2000) *Mol. Microbiol.* **38,** 322–334
10. Jovanoviè, T., Ascenso, C., Hazlett, K. R. O., Sikkink, R., Krebs, C., Litwiller, R., Benson, L. M., Moura, I., Moura, J. J. G., Radolf, J. D., Huynh, B. H., Naylos, S., and Rusnak, F. (2000) *J. Biol. Chem.* **275,** 28439–28448
11. Coulter, E. D., Emerson, J. P., Kurtz, D. M., Jr., and Cabelli, D. E. (2000) *J. Am. Chem. Soc.* **122,** 11555–11556
12. Laemmli, U. K. (1970) *Nature* **227,** 680–685
13. Smith, P. K., Krohn, R. I., Hermanson, G. T., Mallia, A. K., Gartner, F. H., Provenzano, M. D., Fujimoto, E. K., Goeke, N. M., Olson, B. J., and Klenk, D. C. (1985) *Anal. Biochem.* **150,** 76–85
14. Fisher, D. S., and Price, D. C. (1964) *Clin. Chem.* **10,** 21–31
15. McCord, J. M., and Fridovich, I. (1969) *J. Biol. Chem.* **244,** 6049–6055
16. Rush, J. D., and Bielski, B. H. J. (1985) *J. Phys. Chem.* **89,** 5062–5066
17. Schwarz, H. A. (1981) *J. Chem. Ed.* **58,** 101–105
18. Buxton, G. V., Greenstock, C. L., Helman, W. P., and Ross, A. B. (1988) *J. Phys. Chem. Ref. Data* **17,** 676–680
19. Sali, A., and Kuriyan, J. (1999) *Trends Biochem. Sci.* **24,** M20–M24
20. Sánchez, R., Pieper, U., Melo, F., Eswar, N., Martí-Renom, M. A., Madhusudhan, M. S., Mirkovic, N., and Sali, A. (2000) *Nat. Struct. Biol.* **7,** (Suppl.) 986–990
21. Sali, A., and Blundell, T. L. (1993) *J. Mol. Biol.* **234,** 779–815
22. Laskowski, A., MacArthur, M., Moss, D., and Thorton, J. (1993) *J. Appl. Crystallogr.* **26,** 283–291
23. Chen, L., Sharma, P., LeGall, J., Mariano, A. M., Teixeira, M., and Xavier, A. V. (1994) *Eur. J. Biochem.* **226,** 613–618
24. Silva, G., LeGall, J., Xavier, A. V., Teixeira, M., and Rodrigues-Pousada, C. (2001) *J. Bacteriol.* **183,** 4413–4420
25. Wimpenny, J. W. T., and Firth, A. (1972) *J. Bacteriol.* **111,** 24–32
26. Liochev, S. I., and Fridovich, I. (2000) *J. Biol. Chem.* **275,** 38482–38485
27. Lombard, M., Houee-Levin, C., Touati, D., Fontecave, M., and Nivière, V. (2001) *Biochemistry* **40,** 5032–5040
28. Kraulis, P. J. (1991) *J. Appl. Crystallogr.* **24,** 946–950
29. Nicholls, A. (1992) *GRASP: Graphical Representation and Analysis of Surface Properties*, Columbia University, NY
30. Merritt, E. A., and Bacon, D. J. (1997) *Methods Enzymol.* **277,** 505–524